



HAL
open science

Conformational transitions in the active site of mycobacterial 2-oxoglutarate dehydrogenase upon binding phosphonate analogues of 2-oxoglutarate: From a Michaelis-like complex to ThDP adducts

Tristan Wagner, Alexandra Boyko, Pedro Alzari, Victoria Bunik, Marco Bellinzoni

► To cite this version:

Tristan Wagner, Alexandra Boyko, Pedro Alzari, Victoria Bunik, Marco Bellinzoni. Conformational transitions in the active site of mycobacterial 2-oxoglutarate dehydrogenase upon binding phosphonate analogues of 2-oxoglutarate: From a Michaelis-like complex to ThDP adducts. *Journal of Structural Biology*, 2019, 208 (2), pp.182-190. 10.1016/j.jsb.2019.08.012 . pasteur-03095849

HAL Id: pasteur-03095849

<https://pasteur.hal.science/pasteur-03095849>

Submitted on 20 Jul 2022

HAL is a multi-disciplinary open access archive for the deposit and dissemination of scientific research documents, whether they are published or not. The documents may come from teaching and research institutions in France or abroad, or from public or private research centers.

L'archive ouverte pluridisciplinaire **HAL**, est destinée au dépôt et à la diffusion de documents scientifiques de niveau recherche, publiés ou non, émanant des établissements d'enseignement et de recherche français ou étrangers, des laboratoires publics ou privés.



Distributed under a Creative Commons Attribution - NonCommercial 4.0 International License

**Conformational transitions in the active site of mycobacterial 2-oxoglutarate
dehydrogenase upon binding phosphonate analogues of 2-oxoglutarate:
from a Michaelis-like complex to ThDP adducts**

Tristan Wagner^{1#}, Alexandra Boyko², Pedro M. Alzari¹,
Victoria I. Bunik², Marco Bellinzoni^{1*}

¹Unité de Microbiologie Structurale, Institut Pasteur, CNRS, Université de Paris, F-75724
Paris, France

²A.N. Belozersky Institute of Physicochemical Biology and Faculty of Bioengineering and
Bioinformatics, Lomonosov Moscow State University, Russia

Current address: Microbial Metabolism Group, Max Planck Institute for Marine
Microbiology, Celsiusstrasse 1, 28359 Bremen, Germany.

* Corresponding author (marco.bellinzoni@pasteur.fr).

ABSTRACT

Mycobacterial KGD, the thiamine diphosphate (ThDP)-dependent E1 α component of the 2-oxoglutarate dehydrogenase complex (OGDHC), is known to undergo significant conformational changes during catalysis with two distinct conformational states, previously named as the *early* and *late* state. In this work, we employ two phosphonate analogues of 2-oxoglutarate (OG), i.e. succinyl phosphonate (SP) and phosphono ethyl succinyl phosphonate (PESP), as tools to isolate the first catalytic steps and understand the significance of conformational transitions for the enzyme regulation. The kinetics showed a more efficient inhibition of mycobacterial E1 α by SP (K_i 0.043 \pm 0.013 mM) than PESP (K_i 0.88 \pm 0.28 mM), consistent with the different circular dichroism spectra of the corresponding complexes. PESP allowed us to get crystallographic snapshots of the Michaelis-like complex, the first one for 2-oxo acid dehydrogenases, followed by the covalent adduction of the inhibitor to ThDP, mimicking the pre-decarboxylation complex. In addition, covalent ThDP-phosphonate complexes obtained with both compounds by co-crystallization were in the *late* conformational state, probably corresponding to slowly dissociating enzyme-inhibitor complexes. We discuss the relevance of these findings in terms of regulatory features of the mycobacterial E1 α enzymes, and in the perspective of developing tools for species-specific metabolic regulation.

Keywords

2-oxoglutarate dehydrogenase; 2-oxoglutarate phosphonate analogues; *Mycobacterium*; thiamine diphosphate; induced conformational transition

INTRODUCTION

2-Oxoglutarate (OG) is an amphibolic intermediate at a crossroad of carbon and nitrogen metabolism, crucial to energy production in both prokaryotes and eukaryotes (Bunik and Fernie, 2009; Bunik et al., 2013). Irreversible oxidative decarboxylation of OG, carried out by the multienzyme OG dehydrogenase complex (OGDHC), is a highly conserved and regulated process in aerobic organisms (Bunik et al., 2013). OGDHC is a representative of a family of 2-oxoacid dehydrogenase complexes that catalyze oxidative decarboxylation of their specific 2-oxoacid substrates through a multistep process. Final products of the reaction are the high-energy thioester of CoA with the substrate residue (succinyl-CoA in the case of OGDHC), CO₂ and reducing equivalents in the form of NADH.

In the well-characterized OGDHC of different origins, the first enzymatic component (thiamine diphosphate (ThDP)-dependent OG dehydrogenase, or E1o) decarboxylates OG and reductively succinylates the complex-bound lipoyl group. The group is covalently attached to a conserved lysine residue from the lipoyl-bearing domain of the second enzymatic component (dihydrolipoamide succinyltransferase, E2o). The E2o catalytic domain then transfers the dihydrolipoyl-bound succinyl residue to CoA, generating succinyl-CoA and releasing a dihydrolipoyl moiety. The final step is performed by the third component (E3), which reoxidizes the dihydrolipoyl group generating reducing equivalents as NADH. However, in *Corynebacteriales*, the catalytic domains of the OGDHC components E1o and E2o (homologues of *E. coli* SucA and SucB, respectively) are encoded in a single polypeptide, named OdhA in *Corynebacteria* (Usuda et al., 1996) and KGD in *Mycobacteria* (Tian et al., 2005). Since the OdhA/KGD fusion protein has no lipoylated domain, the lipoyl group required for the OGDHC reaction should be provided by the second component of the pyruvate dehydrogenase complex (E2p, dihydrolipoamide acetyltransferase). Owing to this,

OdhA has been proposed to be incorporated into a hybrid complex possessing both the OG and pyruvate dehydrogenase activities (Hoffelder et al., 2010; Wagner et al., 2011). Despite the specific structural organization of the complex, we showed the overall structural similarity of the catalytic E1o domain of *Mycobacterium smegmatis* KGD (Wagner et al., 2011) with the homologue from *Escherichia coli* (*EcSucA*). The latter is the only other E1o enzyme whose crystal structure is so far available, albeit in the apoform (Frank et al., 2007).

The catalytic mechanism of the OG dehydrogenase reaction involves a nucleophilic attack by the ThDP ylide (Fig. 1, violet) on OG, generating a pre-decarboxylation intermediate which is split into CO₂ and a resonance-stabilized α -carbanion / enamine ThDP adduct (Fig. 1, green). The fate of this ThDP-bound decarboxylation intermediate depends on the second substrate of the E1o-catalyzed reaction. In addition to oxidation by the lipoyl domain in the canonical dehydrogenase reaction, the intermediate may be protonated and hydrolyzed generating succinyl semialdehyde (SSA), or undergo carbonylation with glyoxylate resulting in 5-hydroxy-2-oxoadipate (Beigi et al., 2013; Wagner et al., 2011) (Fig. 1, blue). Unlike mammalian OG dehydrogenases, where only the lipoyl-dependent reaction is generally considered to be of physiological relevance, *Mycobacteria* have been shown to rely also on the other two reactions (Balakrishnan et al., 2013; de Carvalho et al., 2010; Tian et al., 2005). In addition, in *Mycobacterium tuberculosis*, KGD (Rv1248c) and its multienzyme complex defend the pathogen against glutamate anaplerosis and/or oxidative and nitrosative stress (Bryk et al., 2002; Maksymiuk et al., 2015), pointing to species-specific roles of the E1o-dependent side reactions involving uncoupled electrons and/or regulatory protein succinylation (Bunik, 2018).

Our previous work on the *M. smegmatis* KGD E1o domain (referred here as *MsSucA*), suggested a reaction mechanism involving large protein motions revealed from snapshots of catalysis *in crystallo* (Wagner et al., 2014). Specifically, we observed two distinct protein

conformations for *MsSucA* in complex with the post-decarboxylation intermediate: an *early* state, in which the enzyme essentially maintains the same conformation observed for the holoenzyme, and a *late* state, where a significant conformational change of the active site is coupled to a 90° rotation of the hydroxybutanoate moiety in the ThDP adduct relative to the thiazole ring plane (Suppl. Fig. S1). The accompanying structural changes in the protein substrate binding site are supposed to be important for increasing reactivity of the *late* state post-decarboxylation adduct towards the acceptor substrate, *i.e.* the lipoyl moiety (Wagner et al., 2011). Whether the *early* and *late* conformational states are common to other E1o enzymes, or rather represent a trait of mycobacterial enzymes, is currently unknown. On the other hand, earlier kinetic studies of the interaction of different ThDP-dependent dehydrogenases and decarboxylases with phosphonate analogues of their substrates revealed slow (with respect to catalytic rates) conformational transitions of the enzyme complexes with the substrate analogues, which are still structurally uncharacterized (reviewed by (Artiukhov et al., 2016; Bunik et al., 2013)). Deciphering the mechanistic details of such transitions could help our ability to tune cellular functions by developing species-specific *in vivo* inhibitors of 2-oxo acid dehydrogenases (Artiukhov et al., 2016). We therefore employed here the phosphonate analogues of OG, such as succinyl phosphonate (SP) and phosphonoethyl succinyl phosphonate (PESP), to resolve conformational transitions of mycobacterial E1o, using *MsSucA* protein as a model of the OG dehydrogenase active site. The *MsSucA*-phosphonate ternary complexes that we describe here provide for the first time structural snapshots of the enzyme Michaelis-like and covalent pre-decarboxylation complexes. Comparison of the ligand orientation and the enzyme conformational state to those observed previously with the natural substrate (Wagner et al., 2014; 2011) sheds new light on the significance of the specific structural states of mycobacterial OG dehydrogenase for catalysis and inhibition.

RESULTS

Interaction of phosphonate analogues of OG with *MsSucA* in solution. SP or its monoethyl ester on the phosphonate group, PESP, are known synthetic analogues of OG where a phosphonate group replaces the leaving carboxyl group (Fig. 2). When the isolated *MsSucA* protein is assayed with artificial electron acceptor 2,6-dichlorophenolindophenol, the phosphonates act as competitive inhibitors of *MsSucA*, increasing the enzyme K_M for OG (Fig. 2, Suppl. Fig. S2). SP is a much stronger inhibitor, compared to PESP, showing a 20-fold difference in the K_i 's (0.043 ± 0.013 mM and 0.88 ± 0.28 mM, respectively). At higher concentrations, SP also significantly decreases the enzyme maximal velocity (Fig. 2), in agreement with similar effect of SP on eukaryotic E1 α , related to the formation of tight, slowly dissociating complexes (Bunik et al., 1992; Bunik and Pavlova, 1993). A more efficient formation of such complexes with the inhibitors upon decreasing the substrate concentrations is probably responsible for an increase in the inhibitory potency of the phosphonates below 0.05 mM OG, leading to strong deviations of the substrate saturation from the hyperbolic kinetics in the presence of SP and PESP. The low substrate concentration range was therefore excluded from our estimation of the relative inhibitory power of SP and PESP by approximation to a hyperbolic substrate saturation or its linear transformations (Suppl. Fig. S2).

The binding of substrates and inhibitors to ThDP-dependent enzymes is known to elicit changes in the enzyme circular dichroism (CD) spectra (Jordan and Nemeria, 2014; Kovina et al., 2004). The CD spectra of the *MsSucA* holoenzyme in the presence of OG and/or its phosphonate analogues indicate that the induced changes in optical rotation are temporary upon the addition of OG and stable upon the addition of SP or PESP (Suppl. Fig. S3A-C). The time-dependent disappearance of the characteristic CD spectra with OG (Suppl. Fig.

S3A) is most likely due to the enzyme-catalyzed non-oxidative decarboxylation of OG, leading to substrate depletion. On a longer time scale, also the OG-induced optical rotation in the presence of PESP returns to the spectrum of the holoenzyme with PESP (Suppl. Fig. S3C). Thus, PESP does not irreversibly block the catalytic consumption of OG, confirming the competitive nature of the interaction of OG and the phosphonates with the *MsSucA* active site.

Differential CD spectra of the optical rotation induced by OG and the phosphonates (Fig. 3) manifest structural differences in the ternary complexes with the substrate and inhibitors. As shown in Fig. 3A, peaks of the differential CD spectra with the phosphonates are shifted to longer wavelengths, compared to OG. Besides, the spectral minimum is more pronounced in the ternary complexes with phosphonates, while the spectral maximum is more pronounced in the ternary complex with OG (Fig. 3A). The maximum amplitude is also higher in the complex with SP than PESP (Fig. 3A). Overall, the CD spectra are consistent with the higher inhibition potency of SP compared to PESP (Suppl. Fig. S2), and the observed differences in the presence of either OG or its phosphonate analogues reflect different conformational states of the *MsSucA* active site and its ThDP adducts.

The protonation of N1' and N4' atoms of the aminopyrimidine ring of ThDP is known to be involved in the optical rotation of ThDP-dependent enzymes in complexes with their substrates or analogues (Kovina et al., 2004; Nemeria et al., 2004; 2007a; 2007b). Indeed, the induced optical rotation in *MsSucA* E952Q point mutant, in which the activation of ThDP is impaired due to the lack of the Glu952 carboxylic group (Fig. 1, purple), differs from that of the wild-type enzyme. Both spectral ellipticity maximum at 265 nm and minimum at 285 nm are far more pronounced upon the E952Q holoenzyme formation, but the spectrum remains invariant upon addition of 1 mM OG (Suppl. Fig. S3D). Surprisingly, the CD spectrum of this point mutant is still sensitive to the addition of SP (Fig. 3B, Suppl. Fig. S3D). In this case,

however, the induced CD changes differ from those observed on the wild-type holoenzyme by a more pronounced maximum at 290 nm and the time dependence of these spectral changes on the minute scale (Fig. 3B). Thus, in contrast to OG, SP can elicit changes in the *MsSucA* ellipticity even when the ThDP ylide formation is significantly slowed down. This finding suggests additional stabilization of the ternary complex of the E952Q mutant *MsSucA* holoenzyme with SP, compared to OG. To further characterize the phosphonates binding mode, we carried out crystallographic studies of *MsSucA* in complex with either SP or PESP.

Phosphonate analogues of OG form covalent adducts with ThDP in *MsSucA*. Crystals of *MsSucA* grown in the presence of 5 mM SP or 5 mM PESP diffract to high resolution (1.6 – 1.7 Å) and belong to the monoclinic space group $P2_1$, different from the *MsSucA* triclinic crystal form described previously ((Wagner et al., 2011); Table 1). The asymmetric unit contains a homodimer, with both protomers found in the enzyme state that we described as the *late* conformation (PDB 2YID, rmsd: 0.24 Å on 714 C α backbone, Suppl. Fig. S4). As expected, both SP and PESP form tetrahedral covalent intermediates with the C₂ atom of ThDP (Fig. 1, red, Fig. 4 and Suppl. Fig. S5), like in similar complexes, obtained upon reaction with methyl acetylphosphonate, in *E. coli* pyruvate dehydrogenase (Arjunan et al., 2006; Kale et al., 2007) or *Lactobacillus plantarum* pyruvate oxidase (Wille et al., 2006).

When each of the two complexes of *MsSucA* holoenzyme with SP or PESP is compared to *MsSucA*-hydroxybutanoate (HB)-ThDP in the *late* conformational state (Wagner et al., 2014) (Suppl. Fig. S5, S6), the HB moiety of the ThDP adduct displays the same orientation and makes equivalent interactions within the active site (Fig. 5A, B and C). In particular, the carboxyl group is coordinated by the imidazolium ring of His579, with the hydroxyl group of Ser604 and a water molecule contacting His539 in both the phosphonate complexes (Fig. 5A, B). Likewise, the active site architecture in the proximity of the different ThDP adducts (Fig. 4) is also essentially invariant when compared to the previously determined structure of the

enzyme in the *late* state. In both cases, the phosphonate groups partially occupy the active site entry channel for the acceptor substrate(s) and are coordinated by salt bridges with the imidazole rings of His747 and His1020 from the opposite monomer (Fig. 5A, B), in addition to hydrogen bonding interactions with two water molecules. It is worth noting that the phosphonate groups of SP or PESP fill into the space that is occupied by the distal carboxylate group of the ThDP adduct in the *early* post-decarboxylation state of the holoenzyme complex with OG (pdb entries 3ZHS and 3ZHT; Suppl. Fig. S1 and S6). Noteworthy, the ethyl group of PESP is accommodated by the hydrophobic environment provided by Phe682, Phe977 and the methyl group from Thr907 (Fig. 4B, 5B).

Time-course soaking experiments with PESP and SP. In our previous work, soaking the OG substrate in triclinic *MsSucA* crystals at 4°C for variable times was key to snapshot different enzyme-ligand complexes of *MsSucA* (Wagner et al., 2014). We therefore tried a similar, time-dependent soaking approach with triclinic *MsSucA* crystals and high concentrations of either SP or PESP (50 mM). In the case of SP, conformations of both the SP-ThDP adduct (Suppl. Fig. S7A) and the enzyme in the resulting complex do not depend on the soaking time. Both are essentially identical to those observed in the cocrystallization experiment (Fig. 4A and Suppl. Fig. S5A), with the *MsSucA*-SP complex adopting the *late* state conformation (rmsd of 0.22 Å on 680 C α backbone). In contrast, soaking PESP does not lead to the formation of a covalent ThDP-bound intermediate at 4°C. Even after protracted soaking (6.5 hours), a non-covalent Michaelis-like complex is observed instead (Fig. 5D and Suppl. Fig. S7B, S8A). The overall architecture of *MsSucA* in this complex corresponds to the enzyme in the *early* state (rmsd of 0.14 Å on 663 C α backbone), which is basically unchanged from the holoenzyme (Wagner et al., 2014), with just minor structural rearrangements in the active site (Suppl. Fig. S8A and C). However, despite the absence of covalent bonding to ThDP and the different conformational state of the enzyme, the bound

PESP exhibits the same relative orientation as in the complex obtained by cocrystallization. Noteworthy, when comparing the PESP soaking complex to the one following short incubations with OG (PDB 3ZHS), both having the enzyme in the same *early* conformation (Fig. 5E), the ethylphosphonate group, oriented perpendicularly to the thiazolium ring, occupies the position which is taken by the distal carboxyl of HB-ThDP (Wagner et al., 2014) (Suppl. Fig. S8). In this *early*, Michaelis-like complex with PESP, His1020 makes polar interactions with the phosphonate and the 2-oxo groups of PESP (Fig. 5D), in agreement with its supposed catalytic role. Indeed, earlier chemical modification studies of animal OG dehydrogenase suggested such interaction of OG with a catalytically essential histidine to increase the reactivity of the C₂ atom of ThDP, in order to help the nucleophilic attack on the substrate by the ThDP ylide (Bunik and Gomazkova, 1996).

Given that soaking PESP at 4°C failed to promote the *early*-to-*late* conformational transition of *MsSucA*, in contrast to the cocrystallization at 18°C, we increased the temperature during the soaking experiments. After 6 min soak with 50 mM PESP at 4°C, *MsSucA* crystals were put at 30°C for 10 min and flash-frozen in liquid nitrogen. Diffraction data at 2.3 Å was obtained for one such crystal (Table 1), showing PESP covalently bound to ThDP in the four crystallographically independent monomers (Suppl. Fig. S7C, S8B). In contrast to the cocrystallization experiment, all the four monomers maintain the *early* post-decarboxylation conformation, like in the previous OG soaking experiment. Yet, some uninterpreted electron density could indicate that a minority of molecules inside the crystals might have undergone a conformational change. Apart from the covalent bond with ThDP, the relative orientation of the now covalent PESP-ThDP adduct does not change from the one observed in the Michaelis-like complex (Suppl. Figs. S7C, S8A and S8B), and so are the interactions with the active site residues (Fig. 5F).

DISCUSSION

Regulatory significance of the conformational transitions of MsSucA. Previous kinetic characterization of the *M. tuberculosis* E1o enzyme suggested that the binding of OG switches the enzyme from a lower to a higher activity state (Balakrishnan et al., 2013). The switch might correspond to the *early* and *late* conformational states shown earlier for the MsSucA holoenzymes in complexes with OG (Wagner et al., 2014; 2011), and here in complexes with the phosphonate inhibitors. It is also known that the binding of allosteric effector acetyl-CoA to mycobacterial E1o increases the enzyme k_{cat} , decreasing both the enzyme K_M for OG and K_i for methyl succinyl phosphonate, a phosphonate analogue similar to PESP (Balakrishnan et al., 2013). Although the ensemble of our structural data shows that the MsSucA transition into the *late* state does not need acetyl-CoA, its binding contributes to stabilizing the *late* post-decarboxylation conformation (Wagner et al., 2011). Altogether, the available data suggest that the *late* conformation of the enzyme may represent its activated state, *i.e.* a state displaying a higher affinity to OG and an increased catalytic rate. According to this view, the *early* and *late* enzyme states might not reflect the consecutive steps of the substrate binding and reductive acylation in the catalytic cycle, but rather an activatory conformational transition. As a consequence, once the product is released, the *late* conformation would not need to return to the *early* state to bind the next substrate molecule. It is worth noting that such activatory transitions of the ThDP-dependent enzymes, which are slow relative to catalysis rates, are known not only for eukaryotic E1o (Bunik et al., 1992), but also for bacterial pyruvate dehydrogenase (Kale et al., 2007) and pyruvate decarboxylase (König, 1998; Kutter et al., 2009; Lu et al., 2000). Analogous transitions of the enzyme-phosphonate complexes may therefore be involved in the formation of the slow dissociating enzyme-inhibitor complexes. Although fully reversible, formation of slow dissociating

complexes may cause decrease in maximal velocity under conditions of kinetic experiments, as we observed with SP (Fig. 2A). In addition, the higher SP potency (K_i 0.043 ± 0.013 mM), when compared to its esterified analogue PESP (K_i 0.88 ± 0.28 mM) (Fig. 2, Suppl. Fig. S2), suggests that the highest affinity of *MsSucA* to these compounds is displayed by the enzyme in the *late* state, as observed by cocrystallization. The more efficient transition of eukaryotic E1o with SP vs. its phosphonomethyl, observed years ago (Bunik et al., 1992), well agrees with the much more pronounced effect of SP vs. PESP on the *MsSucA* maximal velocity reported here (Fig. 2B). The underlying mechanism might involve the steric encumbrance of the PESP ethyl group, whose accommodation by Van der Waals contacts (Fig. 4B, 5D, 5F) may contribute to hindering the conformational transition into a slowly dissociating complex.

Phosphonate analogues of OG as tools to decipher the catalytic steps. Our work provides the first structural evidence of the action of the phosphonate analogues of OG on an E1o active site. The enzyme-inhibitor complexes described here show that the decarboxylation *per se* is not required to trigger the conformational change of the enzyme to the *late* state. On the other hand, the conformational change from the *early* to *late* enzyme state is not required to achieve the decarboxylation either (Wagner et al., 2014), which takes place even in the presence of GarA, the FHA-domain allosteric inhibitor of mycobacterial E1o (Wagner et al., 2019). Unlike the decarboxylation-primed OG, its closest structural analogue SP is rapidly adducted to ThDP (Fig. 4A, Suppl. Fig. S5, S7A), inducing the conformational change of *MsSucA* to what we previously defined as the *late* enzyme state (Suppl. Fig. S1). In contrast, PESP turned out to be an excellent tool to resolve the catalytic steps that precede decarboxylation, most likely due to its less efficient binding to the enzyme (Fig. 2, Suppl. Fig. S2).

The crystallographic snapshots described here suggest that the OG leaving carboxyl group should cover the place occupied by the phosphonate group. It is worth to note that a

similar predecarboxylation mimicking-complex has been resolved for *E. coli* pyruvate dehydrogenase with phosphonolactyl-ThDP (Arjunan et al., 2006). Despite a different active site environment, the X-ray structures show that the orientation of the phosphonate group with respect to ThDP is conserved between the two enzymes (Suppl. Fig. S9). Most notably, in both the SP-ThDP and PESP-ThDP adducts bound to *MsSucA*, the C α -P bond is roughly perpendicular to the thiazolium ring plane, whereas the C α -C $_2$ bond deviates significantly from this same plane (Suppl. Fig. S5), as observed for phosphonolactyl-ThDP bound to *E. coli* E1p (Arjunan et al., 2006). As the orientation of the phosphonate moieties with respect to ThDP is the same in the two enzymes, including in the *MsSucA* Michaelis-like complex with PESP, it is likely to represent the position of the OG leaving carboxyl group at the start of the reaction. On the other hand, the presented data cannot elucidate if the HB-ThDP orientation in the *early* state corresponds to the pre-decarboxylation complex, as suggested earlier (Wagner et al., 2014), or rather follows the protonation of the decarboxylation product in the absence of an acceptor substrate. In view of the multiple physiological roles of mycobacterial E1o, the different conformations of the HB-ThDP adduct could be employed to direct the enzymatic reaction through the different pathways (Fig. 1, blue).

Significance for metabolic regulation. Our structural insights help deciphering mechanisms of the complex interaction of this class of potent synthetic inhibitors of ThDP-dependent OG dehydrogenases, which act with high selectivity *in vivo*. Multiple studies of mammalian systems have demonstrated that the phosphonate analogues of OG may have a pronounced metabolic impact with cell-specific signatures (Allen et al., 2016; Bunik, 2017; Ilic et al., 2017). On the other hand, *in vitro* experiments on *M. tuberculosis* did not reveal any significant growth inhibition by SP or PESP (Fang et al., 2010), presumably due to the poor penetration of the charged compounds through the mycobacterial cell wall. Given the features of the mycobacterial E1o enzymes, however, and their complex allosteric regulation

(Balakrishnan et al., 2013; Wagner et al., 2019; 2011), it cannot be excluded that the antibiotic effect of the analogues might increase under specific conditions. It is indeed known that *M. tuberculosis* E1o is part of a regulatory circuit centered on GarA, whose phosphorylation state regulates the carbon flux between the TCA cycle and glutamate metabolism (Rieck et al., 2017; Ventura et al., 2013; Wagner et al., 2019). Our structural work is therefore a first step to create species-specific synthetic inhibitors of OG dehydrogenases, based on the enzyme conformational transitions, because the residues involved in interactions with phosphonates in *MsSucA* are conserved within all clades (Suppl. Fig. S10). Independent of the species-specific action, such inhibitors may be employed for extending our knowledge on physiological adaptation mechanisms and metabolic rerouting.

MATERIALS AND METHODS

Protein production and mutagenesis

Recombinant *MsSucA* corresponds to residues 361-1227 of the OdhA protein from *Mycobacterium smegmatis*. *MsSucA* was expressed in *E. coli* and purified as described previously (Wagner et al., 2011); the inactive point mutant E952Q was expressed in the same conditions from a variant pET-28a/*MsSucA* expression plasmid, in which the mutation was introduced by the QuickChange mutagenesis method (Agilent), and purified as the wild-type enzyme. Sodium salts of the phosphonate analogues of OG (SP and PESP) were synthesized as described previously (Bunik et al., 2005).

Enzymatic activity measurements

The determination of oxidative OG decarboxylation activity was performed using the artificial two-electron acceptor 2,6-dichlorophenolindophenol (Bunik et al., 2010). When

oxidized, this dye has an absorbance peak at 600 nm, and its reduction into colorless form by the post-decarboxylation enamine-ThDP intermediate leads to a decrease in absorbance. The reaction was therefore followed by the decrease of absorbance of oxidized 2,6-dichlorophenolindophenol at 600 nm at 26°C using a CLARIOstar microplate reader (BMG Labtech, Germany). The reaction medium contained 0.1 M KH_2PO_4 buffer pH 7.0, 1 mM ThDP, 1 mM MgCl_2 and 0.15 mM 2,6-dichlorophenolindophenol. The concentrations of phosphonate analogues varied from 0 to 5 mM, and those of OG from 0 to 2 mM. The reaction was started by addition of reaction medium to a well containing separated drops of OG, a phosphonate analogue and 0.15 μM *MsSucA*. The linear region of the progress curves was used to calculate the steady state velocities. Blank reaction rate was measured in the reaction medium omitting OG. The measurements were performed in triplicate.

Circular dichroism

Measurements were performed at 30°C using a CD 215 spectropolarimeter (Aviv) flushed with N_2 in the range from 250 to 330 nm using a 1 cm cell. Protein samples were dialyzed against a buffer containing 25 mM Tris-HCl pH 7.6, 150 mM NaCl, and diluted to a final concentration of 1 mg/ml. Before starting the experiments, the protein was supplemented with 1 mM MgCl_2 , 0.1 mM ThDP, 0.1/1.0 mM OG and 5 mM of either phosphonate, as stated in the figure legends.

Crystallization and X-ray crystallography

Crystal growth was performed by the hanging drop vapor-diffusion method as described (Wagner et al., 2011). Monoclinic crystals of *MsSucA* in the presence of 5 mM SP or 5 mM PESP were grown at 18°C using 2% 2-methyl-2-propanol, 47% MPD. For cryo-trapping experiments, well-diffracting triclinic crystals of *MsSucA* were grown at 4°C using 25 mg/mL

of the enzyme supplemented with 2 mM ThDP and 5 mM MgCl₂ in 52% to 59% 2-methyl-2,4-pentanediol, 22-25 mM sodium acetate. These triclinic *MsSucA* crystals were soaked in the crystallization solution supplemented with 50 mM SP or 50 mM PESP at the temperatures indicated. All diffraction datasets were collected from single crystals at 100 K using synchrotron radiation either at the ESRF (Grenoble, France) or SOLEIL (Saint-Aubin, France). Data were processed with autoPROC (Vonnrhein et al., 2011) or by stand-alone XDS (Kabsch, 2010), and scaled with SCALA/AIMLESS from the CCP4 suite (Winn et al., 2011). The crystal structures were solved by molecular replacement using the available coordinates of *MsSucA* in either the *early* (pdb entry 2YIC) or the *late* conformational state (pdb entry 2YID) without ligands and solvent as the search models. All models were then manually rebuilt with COOT (Emsley et al., 2010) and further refined with BUSTER, applying local structure similarity restraints for non-crystallography symmetry (NCS) (Smart et al., 2012) and a translation libration screw (TLS) model. Data collection, refinement statistics and pdb entry codes for deposited models and structure factors are reported in Table 1. Figures were generated and rendered with PyMol (Schrödinger, LLC., 2012).

Accession numbers

Coordinates and structure factors of all *MsSucA* complexes described in this work have been deposited to the Protein Data Bank under the following IDs: 6R29, SP cocrystallization; 6R2A, PESP cocrystallization; 6R2B, SP soaking; 6R2C, PESP short soaking; 6R2D, PESP soaking followed by temperature increase (30°C).

ACKNOWLEDGEMENTS

We are grateful to Bruno Baron (Molecular Biophysics Platform, Institut Pasteur) for his helpful assistance with circular dichroism experiments, and to Ahmed Haouz and Patrick

Weber (Crystallography Platform, Institut Pasteur) for carrying out robot-driven crystallization screenings. We acknowledge the synchrotron sources Soleil (Saint-Aubin, France) and ESRF (Grenoble, France) for granting access to their facilities, and their staff for helpful assistance on the respective beamlines. This work was partially supported by institutional grants from the Institut Pasteur and the CNRS. VIB greatly acknowledges current financial support of the work of her group on the phosphonates by RSCF grant 18-14-00116.

REFERENCES

- Allen, E.L., Ulanet, D.B., Pirman, D., Mahoney, C.E., Coco, J., Si, Y., Chen, Y., Huang, L., Ren, J., Choe, S., Clasquin, M.F., Artin, E., Fan, Z.P., Cianchetta, G., Murtie, J., Dorsch, M., Jin, S., Smolen, G.A., 2016. Differential aspartate usage identifies a subset of cancer cells particularly dependent on OGDH. *Cell Reports* 17, 876–890. doi:10.1016/j.celrep.2016.09.052
- Arjunan, P., Sax, M., Brunskill, A., Chandrasekhar, K., Nemeria, N., Zhang, S., Jordan, F., Furey, W., 2006. A thiamin-bound, pre-decarboxylation reaction intermediate analogue in the pyruvate dehydrogenase E1 subunit induces large scale disorder-to-order transformations in the enzyme and reveals novel structural features in the covalently bound adduct. *J. Biol. Chem.* 281, 15296–15303. doi:10.1074/jbc.M600656200
- Artiukhov, A.V., Graf, A.V., Bunik, V.I., 2016. Directed regulation of multienzyme complexes of 2-oxo acid dehydrogenases using phosphonate and phosphinate analogs of 2-oxo acids. *Biochemistry Mosc.* 81, 1498–1521. doi:10.1134/S0006297916120129
- Balakrishnan, A., Jordan, F., Nathan, C.F., 2013. Influence of allosteric regulators on individual steps in the reaction catalyzed by *Mycobacterium tuberculosis* 2-hydroxy-3-oxoadipate synthase. *J. Biol. Chem.* 288, 21688–21702. doi:10.1074/jbc.M113.465419

- Beigi, M., Loschonsky, S., Lehwald, P., Brecht, V., Andrade, S.L.A., Leeper, F.J., Hummel, W., Müller, M., 2013. α -Hydroxy- β -keto acid rearrangement-decarboxylation: impact on thiamine diphosphate-dependent enzymatic transformations. *Org. Biomol. Chem.* 11, 252–256. doi:10.1039/c2ob26981c
- Bryk, R., Lima, C.D., Erdjument-Bromage, H., Tempst, P., Nathan, C., 2002. Metabolic enzymes of mycobacteria linked to antioxidant defense by a thioredoxin-like protein. *Science* 295, 1073–1077. doi:10.1126/science.1067798
- Bunik, V., 2018. Redox-driven signaling: 2-oxo acid dehydrogenase complexes as sensors and transmitters of metabolic imbalance. *Antioxid. Redox Signal.* ars.2017.7311. doi:10.1089/ars.2017.7311
- Bunik, V., 2017. Vitamin-dependent multienzyme complexes of 2-oxo acid dehydrogenases. Nova Science Publishers, Hauppauge, NY, USA.
- Bunik, V.I., Biryukov, A.I., Zhukov, Y.N., 1992. Inhibition of pigeon breast muscle α -ketoglutarate dehydrogenase by phosphonate analogues of α -ketoglutarate. *FEBS Lett.* 303, 197–201. doi:10.1016/0014-5793(92)80518-L
- Bunik, V.I., Denton, T.T., Xu, H., Thompson, C.M., Cooper, A., Gibson, G.E., 2005. Phosphonate analogues of alpha-ketoglutarate inhibit the activity of the alpha-ketoglutarate dehydrogenase complex isolated from brain and in cultured cells. *Biochemistry* 44, 10552–10561. doi:10.1021/bi0503100
- Bunik, V.I., Fernie, A.R., 2009. Metabolic control exerted by the 2-oxoglutarate dehydrogenase reaction: a cross-kingdom comparison of the crossroad between energy production and nitrogen assimilation. *Biochem. J.* 422, 405–421. doi:10.1042/BJ20090722
- Bunik, V.I., Gomazkova, V.S., 1996. Study of 2-oxoglutarate dehydrogenase by the method of chemical modification of amino acid residues, in: Kurganov, B.I., Nagradova, N.K.,

- Lavrik, O.I. (Eds.), *Chemical Modification of Enzymes*. Nova Science Publishers, New York, pp. 479–521.
- Bunik, V.I., Pavlova, O.G., 1993. Inactivation of alpha-ketoglutarate dehydrogenase during oxidative decarboxylation of alpha-ketoadipic acid. *FEBS Lett.* 323, 166–170.
doi:10.1016/0014-5793(93)81472-c
- Bunik, V.I., Raddatz, G., Strumilo, S., 2013. Translating enzymology into metabolic regulation: the case of the 2-oxoglutarate dehydrogenase multienzyme complex. *Curr. Chem. Biol.* 7, 74–93. doi:10.2174/2212796811307010008
- Bunik, V.I., Schloss, J.V., Pinto, J.T., Dudareva, N., Cooper, A.J.L., 2010. A survey of oxidative paracatalytic reactions catalyzed by enzymes that generate carbanionic intermediates: Implications for ROS production, cancer etiology, and neurodegenerative diseases. *Adv. Enzymol. Relat. Areas Mol. Biol.* 77, 307–360.
- de Carvalho, L.P.S., Zhao, H., Dickinson, C.E., Arango, N.M., Lima, C.D., Fischer, S.M., Ouerfelli, O., Nathan, C., Rhee, K.Y., 2010. Activity-based metabolomic profiling of enzymatic function: identification of Rv1248c as a mycobacterial 2-hydroxy-3-oxoadipate synthase. *Chem. Biol.* 17, 323–332. doi:10.1016/j.chembiol.2010.03.009
- Emsley, P., Lohkamp, B., Scott, W.G., Cowtan, K., 2010. Features and development of Coot. *Acta Crystallogr D Biol Crystallogr* 66, 486–501. doi:10.1107/S0907444910007493
- Fang, M., Toogood, R.D., Macova, A., Ho, K., Franzblau, S.G., McNeil, M.R., Sanders, D.A.R., Palmer, D.R.J., 2010. Succinylphosphonate esters are competitive inhibitors of MenD that show active-site discrimination between homologous alpha-ketoglutarate-decarboxylating enzymes. *Biochemistry* 49, 2672–2679. doi:10.1021/bi901432d
- Frank, R.A.W., Price, A.J., Northrop, F.D., Perham, R.N., Luisi, B.F., 2007. Crystal structure of the E1 component of the Escherichia coli 2-oxoglutarate dehydrogenase multienzyme complex. *J. Mol. Biol.* 368, 639–651. doi:10.1016/j.jmb.2007.01.080

- Hoffelder, M., Raasch, K., van Ooyen, J., Eggeling, L., 2010. The E2 domain of OdhA of *Corynebacterium glutamicum* has succinyltransferase activity dependent on lipoyl residues of the acetyltransferase AceF. *J. Bacteriol.* 192, 5203–5211.
doi:10.1128/JB.00597-10
- Ilic, N., Birsoy, K., Aguirre, A.J., Kory, N., Pacold, M.E., Singh, S., Moody, S.E., DeAngelo, J.D., Spardy, N.A., Freinkman, E., Weir, B.A., Tsherniak, A., Cowley, G.S., Root, D.E., Asara, J.M., Vazquez, F., Widlund, H.R., Sabatini, D.M., Hahn, W.C., 2017. PIK3CA mutant tumors depend on oxoglutarate dehydrogenase. *Proc. Natl. Acad. Sci. USA* 114, E3434–E3443. doi:10.1073/pnas.1617922114
- Jordan, F., Nemeria, N.S., 2014. Progress in the experimental observation of thiamin diphosphate-bound intermediates on enzymes and mechanistic information derived from these observations. *Bioorg. Chem.* 57, 251–262. doi:10.1016/j.bioorg.2014.08.002
- Kabsch, W., 2010. XDS. *Acta Crystallogr. D Biol. Crystallogr.* 66, 125–132.
doi:10.1107/S0907444909047337
- Kale, S., Arjunan, P., Furey, W., Jordan, F., 2007. A dynamic loop at the active center of the *Escherichia coli* pyruvate dehydrogenase complex E1 component modulates substrate utilization and chemical communication with the E2 component. *J. Biol. Chem.* 282, 28106–28116. doi:10.1074/jbc.M704326200
- Kovina, M.V., de Kok, A., Sevostyanova, I.A., Khailova, L.S., Belkina, N.V., Kochetov, G.A., 2004. The molecular origin of the thiamine diphosphate-induced spectral bands of ThDP-dependent enzymes. *Proteins* 56, 338–345. doi:10.1002/prot.20115
- König, S., 1998. Subunit structure, function and organisation of pyruvate decarboxylases from various organisms. *Biochim. Biophys. Acta* 1385, 271–286.

- Kutter, S., Weiss, M.S., Wille, G., Golbik, R., Spinka, M., König, S., 2009. Covalently bound substrate at the regulatory site of yeast pyruvate decarboxylases triggers allosteric enzyme activation. *J. Biol. Chem.* 284, 12136–12144. doi:10.1074/jbc.M806228200
- Lu, G., Dobritzsch, D., Baumann, S., Schneider, G., König, S., 2000. The structural basis of substrate activation in yeast pyruvate decarboxylase. A crystallographic and kinetic study. *Eur. J. Biochem.* 267, 861–868.
- Maksymiuk, C., Balakrishnan, A., Bryk, R., Rhee, K.Y., Nathan, C.F., 2015. E1 of α -ketoglutarate dehydrogenase defends *Mycobacterium tuberculosis* against glutamate anaplerosis and nitroxidative stress. *Proc. Natl. Acad. Sci. USA* 112, E5834–43. doi:10.1073/pnas.1510932112
- Nemeria, N., Baykal, A., Joseph, E., Zhang, S., Yan, Furey, W., Jordan, F., 2004. Tetrahedral Intermediates in thiamin diphosphate-dependent decarboxylations exist as a 1',4'-imino tautomeric form of the coenzyme, unlike the Michaelis complex or the free coenzyme. *Biochemistry* 43, 6565–6575. doi:10.1021/bi049549r
- Nemeria, N., Chakraborty, S., Baykal, A., Korotchkina, L.G., Patel, M.S., Jordan, F., 2007a. The 1',4'-iminopyrimidine tautomer of thiamin diphosphate is poised for catalysis in asymmetric active centers on enzymes. *Proc. Natl. Acad. Sci. USA* 104, 78–82. doi:10.1073/pnas.0609973104
- Nemeria, N., Korotchkina, L., McLeish, M.J., Kenyon, G.L., Patel, M.S., Jordan, F., 2007b. Elucidation of the chemistry of enzyme-bound thiamin diphosphate prior to substrate binding: defining internal equilibria among tautomeric and ionization states. *Biochemistry* 46, 10739–10744. doi:10.1021/bi700838q
- Rieck, B., Degiacomi, G., Zimmermann, M., Cascioferro, A., Boldrin, F., Lazar-Adler, N.R., Bottrill, A.R., Le Chevalier, F., Frigui, W., Bellinzoni, M., Lisa, M.-N., Alzari, P.M., Nguyen, L., Brosch, R., Sauer, U., Manganelli, R., O'Hare, H.M., 2017. PknG senses

- amino acid availability to control metabolism and virulence of *Mycobacterium tuberculosis*. PLoS Pathog. 13, e1006399. doi:10.1371/journal.ppat.1006399
- Schrödinger, LLC., 2012. The PyMOL Molecular Graphics System.
- Smart, O.S., Womack, T.O., Flensburg, C., Keller, P., Paciorek, W., Sharff, A., Vornrhein, C., Bricogne, G., 2012. Exploiting structure similarity in refinement: automated NCS and target-structure restraints in BUSTER. Acta Crystallogr. D Biol. Crystallogr. 68, 368–380. doi:10.1107/S0907444911056058
- Tian, J., Bryk, R., Itoh, M., Suematsu, M., Nathan, C., 2005. Variant tricarboxylic acid cycle in *Mycobacterium tuberculosis*: identification of alpha-ketoglutarate decarboxylase. Proc. Natl. Acad. Sci. USA 102, 10670–10675. doi:10.1073/pnas.0501605102
- Usuda, Y., Tujimoto, N., Abe, C., Asakura, Y., Kimura, E., Kawahara, Y., Kurahashi, O., Matsui, H., 1996. Molecular cloning of the *Corynebacterium glutamicum* (“*Brevibacterium lactofermentum*” AJ12036) *odhA* gene encoding a novel type of 2-oxoglutarate dehydrogenase. Microbiology 142, 3347–3354.
- Ventura, M., Rieck, B., Boldrin, F., Degiacomi, G., Bellinzoni, M., Barilone, N., Alzaidi, F., Alzari, P.M., Manganelli, R., O'Hare, H.M., 2013. GarA is an essential regulator of metabolism in *Mycobacterium tuberculosis*. Mol. Microbiol. 90, 356–366. doi:10.1111/mmi.12368
- Vornrhein, C., Flensburg, C., Keller, P., Sharff, A., Smart, O., Paciorek, W., Womack, T., Bricogne, G., 2011. Data processing and analysis with the autoPROC toolbox. Acta Crystallogr. D Biol. Crystallogr. 67, 293–302. doi:10.1107/S0907444911007773
- Wagner, T., Andre-Leroux, G., Hindie, V., Barilone, N., Lisa, M.-N., Hoos, S., Raynal, B., Vulliez-Le Normand, B., O'Hare, H.M., Bellinzoni, M., Alzari, P.M., 2019. Structural insights into the functional versatility of an FHA domain protein in mycobacterial signaling. Science Signaling 12. doi:10.1126/scisignal.aav9504

- Wagner, T., Barilone, N., Alzari, P.M., Bellinzoni, M., 2014. A dual conformation of the post-decarboxylation intermediate is associated with distinct enzyme states in mycobacterial KGD (α -ketoglutarate decarboxylase). *Biochem. J.* 457, 425–434. doi:10.1042/BJ20131142
- Wagner, T., Bellinzoni, M., Wehenkel, A., O'Hare, H.M., Alzari, P.M., 2011. Functional plasticity and allosteric regulation of α -ketoglutarate decarboxylase in central mycobacterial metabolism. *Chem. Biol.* 18, 1011–1020. doi:10.1016/j.chembiol.2011.06.004
- Wille, G., Meyer, D., Steinmetz, A., Hinze, E., Golbik, R., Tittmann, K., 2006. The catalytic cycle of a thiamin diphosphate enzyme examined by cryocrystallography. *Nat. Chem. Biol.* 2, 324–328. doi:10.1038/nchembio788
- Winn, M.D., Ballard, C.C., Cowtan, K.D., Dodson, E.J., Emsley, P., Evans, P.R., Keegan, R.M., Krissinel, E.B., Leslie, A.G.W., McCoy, A., McNicholas, S.J., Murshudov, G.N., Pannu, N.S., Potterton, E.A., Powell, H.R., Read, R.J., Vagin, A., Wilson, K.S., 2011. Overview of the CCP4 suite and current developments. *Acta Crystallogr. D Biol. Crystallogr.* 67, 235–242. doi:10.1107/S0907444910045749

FIGURE LEGENDS

Figure 1. *MsSucA* reaction scheme. Background colors refer to the different reaction steps: ThDP activation (purple), OG decarboxylation (green), end products according to the three alternative reaction outcomes (carbonylation, reductive acylation or non-reductive decarboxylation; blue), phosphonate binding and inhibition (light red). R1: b-hydroxyethylidiphosphate; R2: 4'-amino-2-methyl-5-pyrimidyl; R3: propanoate.

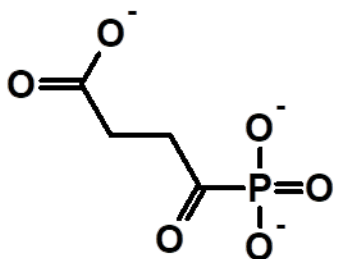
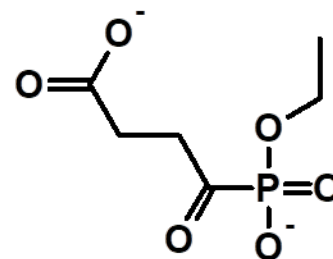
Figure 2. Inhibition of *MsSucA* by the phosphonate analogues. SP (**A**) or PESP (**B**) were added to 0.15 μ M *MsSucA* at the concentrations 0.05 mM, 0.2 mM, 0.5 mM, and 5 mM. The reactions were started by adding the reaction medium to the wells comprising separate drops of OG, a phosphonate analogue and the protein. The reactions were followed by the decrease in absorbance upon reduction of the artificial electron acceptor 2,6-dichlorophenolindophenol (0.15 mM) at 600 nm. Data are presented as mean \pm SEM in the semilogarithmic scale, their fitting by hyperbolic function using Michaelis-Menten equation is shown in insets, with the approximation parameters provided in Suppl. Fig. S2.

Figure 3. Changes in *MsSucA* circular dichroism (CD) spectra after addition of OG and its phosphonate analogues. (**A**) Differential CD spectra of the *MsSucA* holoenzyme incubated with 0.1 mM OG (yellow), 5 mM SP (red) or 5 mM PESP (blue) for 1 minute at 30°C. (**B**) Differential CD spectra of *MsSucA* E952Q (holoenzyme) incubated with 1 mM OG (green) or 5 mM SP for 1 minute (light purple) or 5 minutes (purple) at 30°C. For comparison, differential CD spectra for wild type *MsSucA* holoenzyme incubated with 5 mM SP for 1 minute (red) is also given in (**B**). Differential spectra are obtained by subtraction of the CD spectrum of *MsSucA* incubated with 1 mM MgCl₂ and 0.1 mM ThDP at 30°C from the CD

spectrum of the holoenzyme in the same conditions with addition of OG or phosphonates as described above.

Figure 4. Active site coordination of ThDP-phosphonate covalent adducts. Stereo view of the coordination, inside the *MsSucA* active site, of the ThDP covalent adducts formed upon cocrystallization with SP (**A**) and PESP (**B**). Cyan and blue colors indicate the residues belonging to the two different *MsSucA* protomers; residues shown in pink (Phe682, Thr907 and Phe977) interact with the PESP ethyl group.

Figure 5. *MsSucA* catalytic snapshots. Active site interactions of ThDP covalent adducts in *MsSucA*, following reaction with the phosphonate analogues SP and PESP (this work) or the natural substrate OG (Wagner et al., 2014). (**A**) ThDP-SP following cocrystallization; (**B**) ThDP-PESP following cocrystallization; (**C**) HB-ThDP following long soakings with OG, as described (pdb entry 2YIC); (**D**) PESP Michaelis-Menten complex obtained by inhibitor soaking; (**E**) HB-ThDP following short soakings with OG (pdb entry 3ZHS); (**F**) ThDP-PESP following soaking and temperature increase to 30°C for 6 min (see text). Blue, dotted lines indicate hydrogen bond or salt bridge interactions, with values providing atomic distances in Å (averaged over all molecules in the asymmetric unit). Van der Waals interactions are indicated by a brown, wavy line.

A**SP****B****PESP**

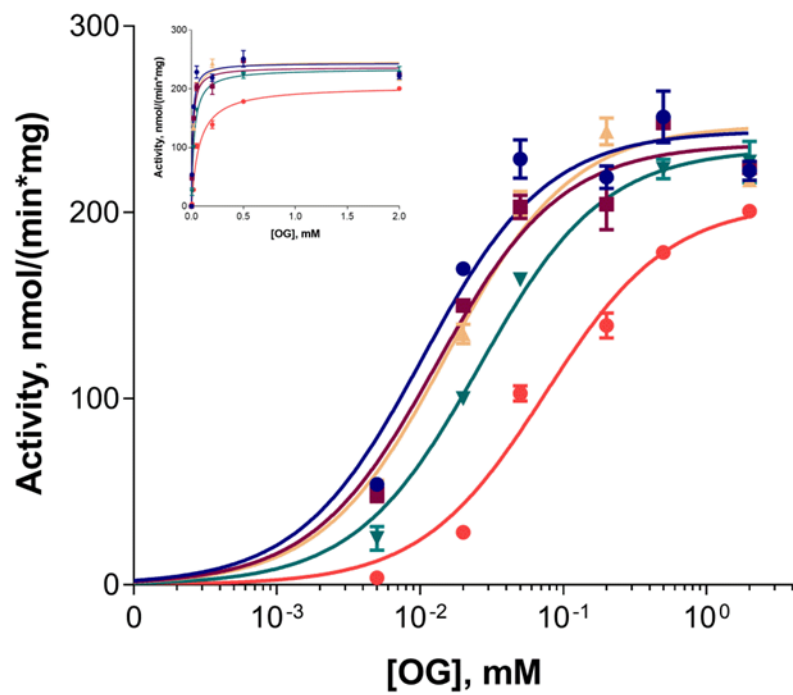
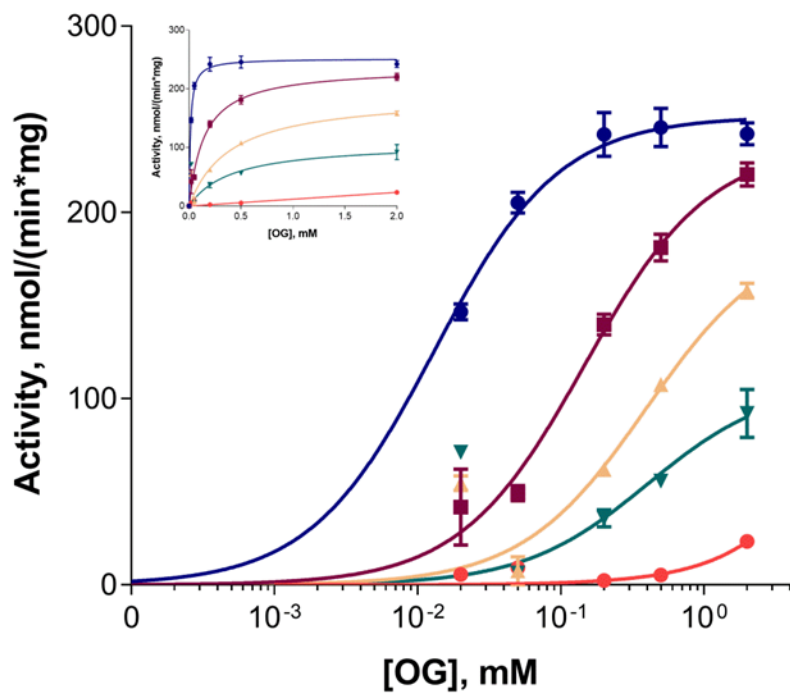
● 0 mM

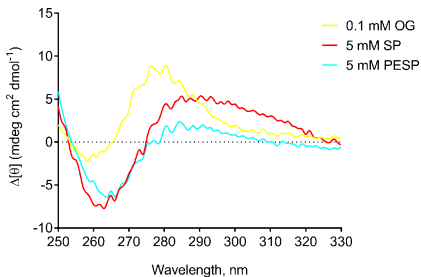
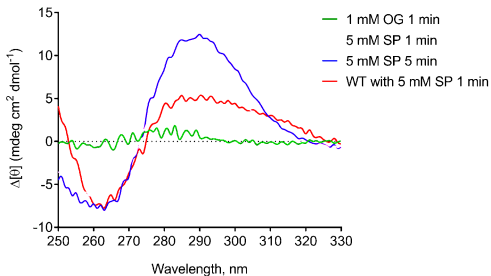
■ 0.05 mM

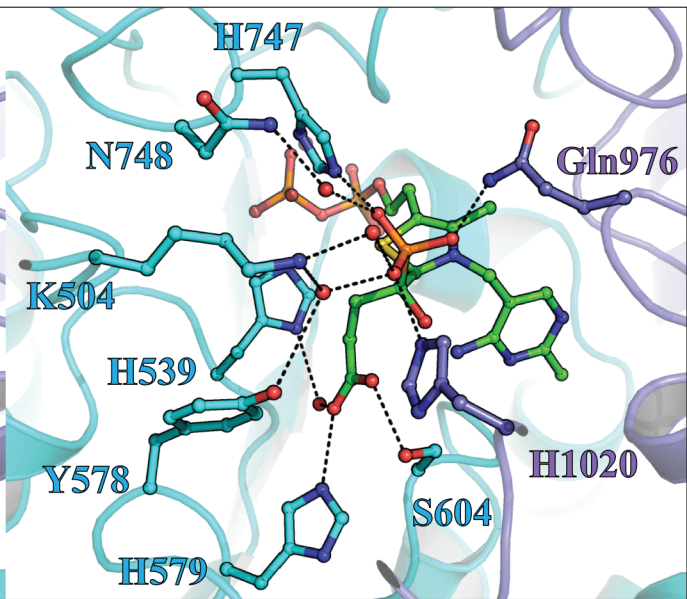
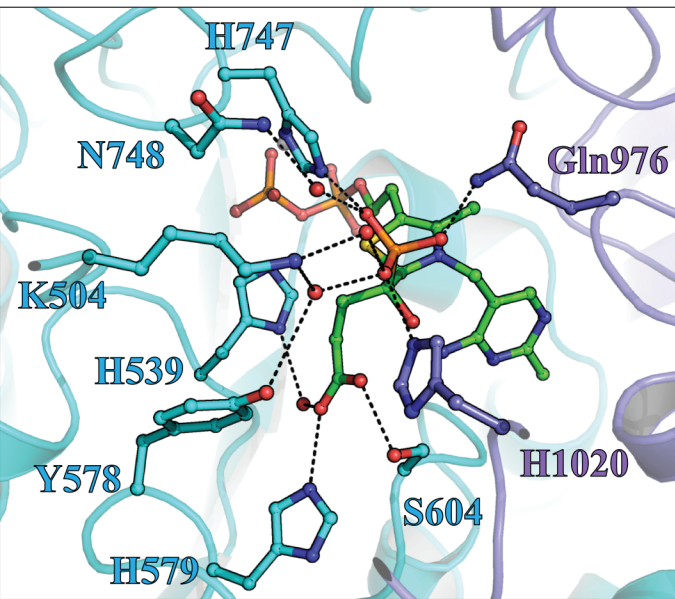
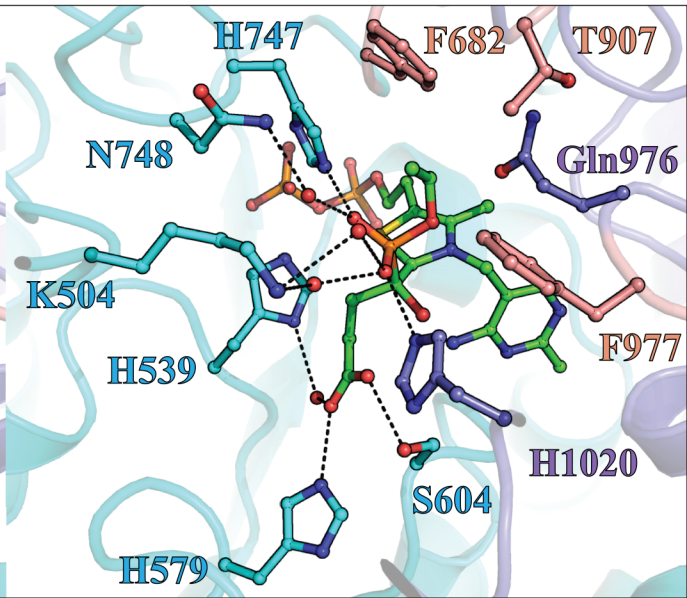
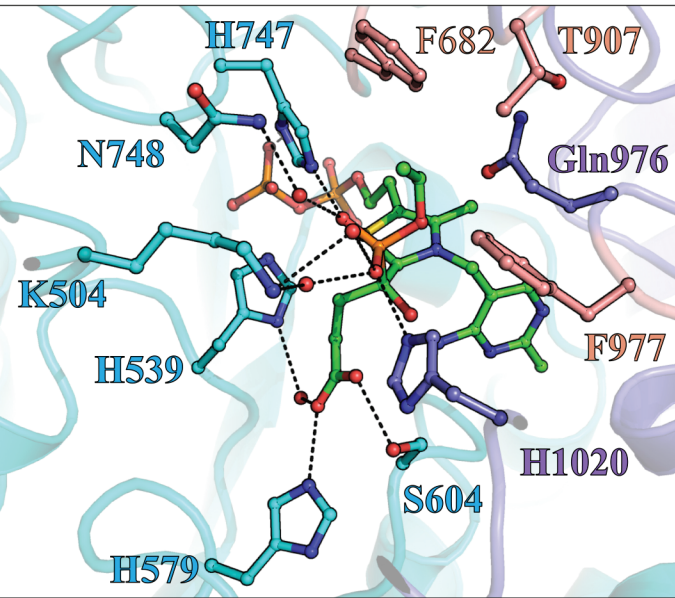
▲ 0.2 mM

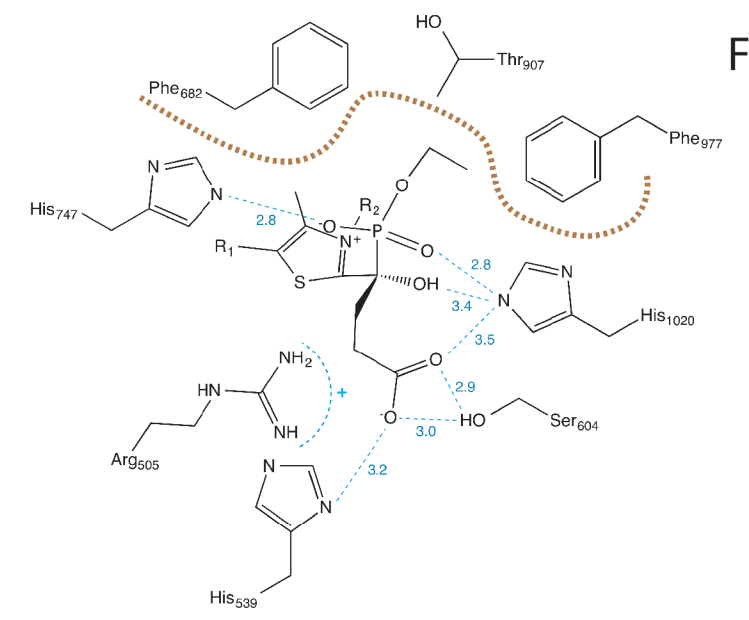
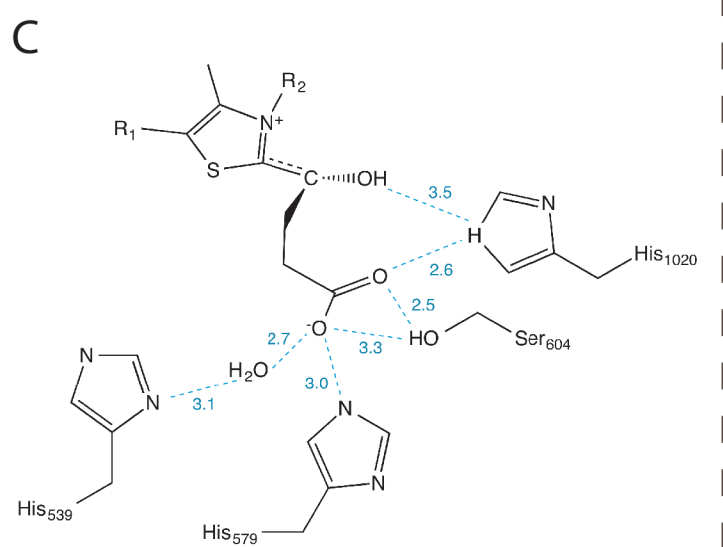
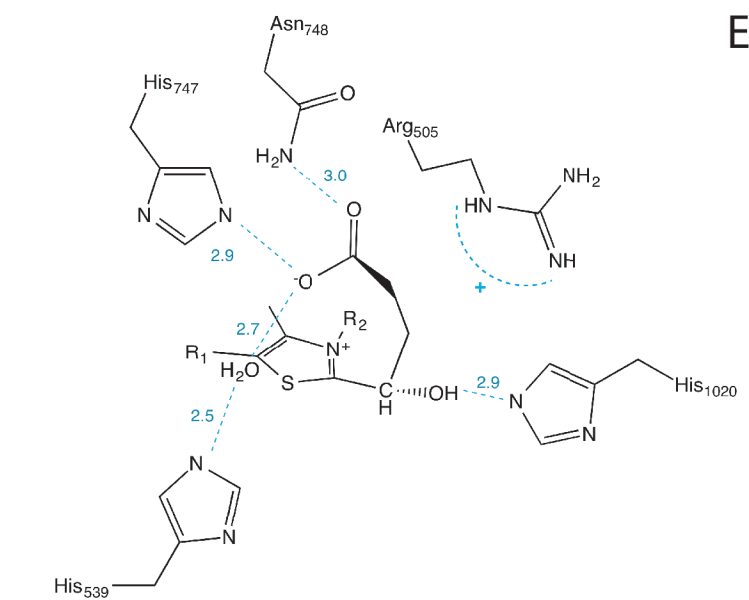
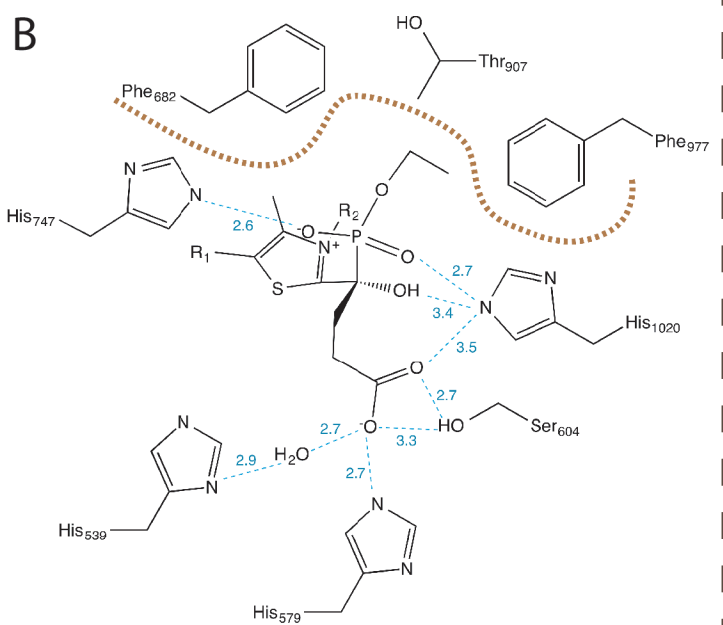
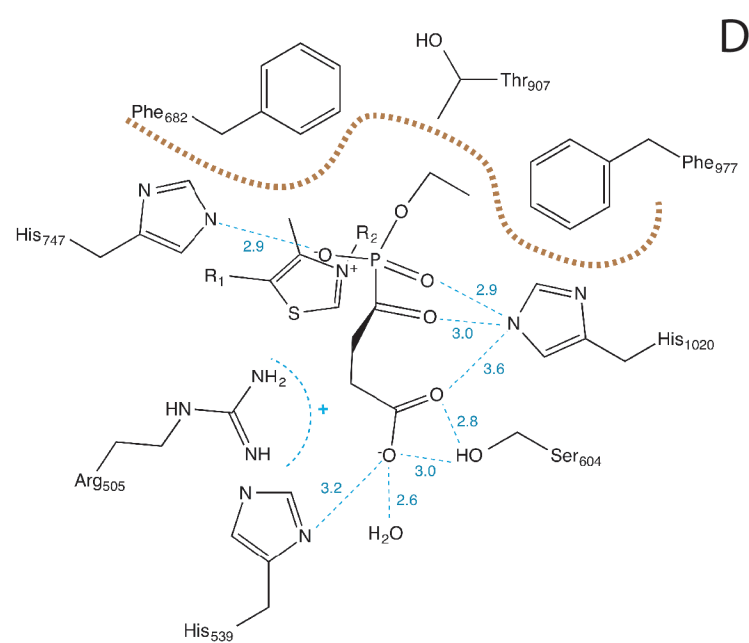
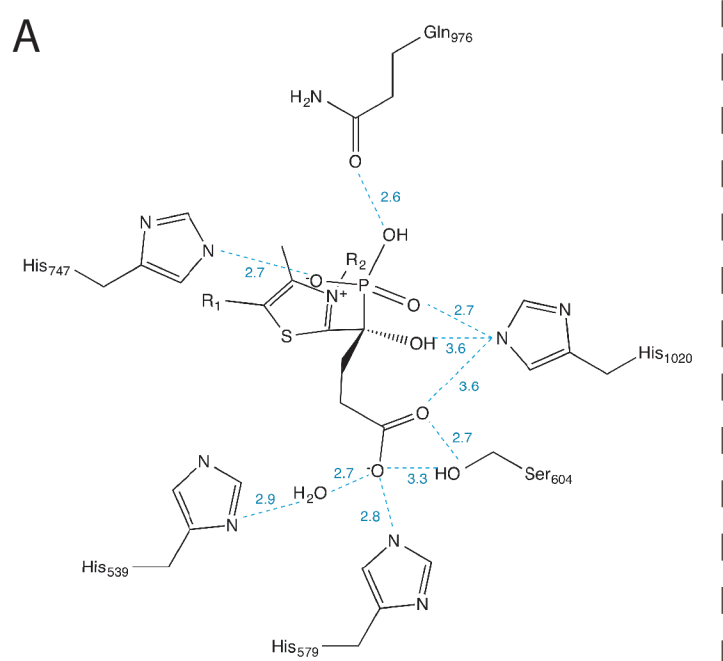
▼ 0.5 mM

● 5 mM



A**B**

A**B**



Data collection	SP cocrystallization	PESP cocrystallization	SP soaking	PESP short soaking	PESP soaking + temperature increase
Synchrotron beamline	SOLEIL Proxima 1	ESRF ID14-4	SOLEIL Proxima 1	SOLEIL Proxima 1	SOLEIL Proxima 1
Wavelength (Å)	0.98011	0.9393	0.97895	0.97895	0.98011
Space group	P2 ₁	P2 ₁	P1	P1	P1
Cell dimensions <i>a, b, c</i> (Å)	86.47, 108.17, 120.54	86.48, 108.02, 120.53	82.12, 82.76, 162.97	81.40, 83.96, 160.68	80.84, 83.73, 160.58
α, β, γ (°)	90, 103.78, 90	90, 103.55, 90	98.55, 97.52, 102.18	99.54, 98.78, 100.89	99.52, 98.94, 100.81
Resolution (Å)	117.07 – 1.67 (1.69 – 1.67)	40.37 – 1.70 (1.79 – 1.70)	158.88 – 1.96 (2.00 – 1.96)	78.48 – 2.09 (2.12 – 2.10)	77.92 – 2.30 (2.34 – 2.30)
<i>R</i> _{merge}	0.099 (0.780)	0.065 (0.458)	0.076 (0.503)	0.070 (0.565)	0.056 (0.465)
<i>I</i> / $\sigma(I)$	9.9 (2.1)	11.8 (2.4)	8.6 (2.1)	10.0 (2.2)	10.2 (2.1)
Completeness (%)	99.7 (99.3)	98.6 (95.7)	97.1 (96.6)	97.4 (96.4)	97.2 (97.2)
CC(1/2)	0.993 (0.734)	0.996 (0.792)	0.995 (0.800)	0.997 (0.830)	0.997 (0.804)
Redundancy	5.7 (5.8)	3.3 (2.7)	2.9 (3.0)	2.9 (2.8)	2.9 (2.9)
Refinement					
Resolution (Å)	1.67	1.70	1.96	2.09	2.30
No. reflections	250496	232481	284471	233039	171953
<i>R</i> _{work} / <i>R</i> _{free} (%)	15.3 / 16.3	15.1 / 16.8	22.8 / 24.5	23.2 / 24.6	21.7 / 24.2
No. atoms					
Protein	13305	13296	26203	25237	25045
Ligand/ions	118	130	156	164	164
Solvent	1277	1269	1360	847	997
Average B-factors					
Protein	32.4	31.1	33.5	43.7	58.8
Ligand/ions	29.9	31.6	22.2	32.9	46.0
Solvent	40.4	37.7	31.4	35.2	52.1
R.m.s deviations					
Bond lengths (Å)	0.010	0.010	0.010	0.009	0.010
Bond angles (°)	0.95	0.93	0.98	0.94	1.04
PDB	6R29	6R2A	6R2B	6R2C	6R2D

Table 1. Crystallographic data collection and refinement statistics (highest resolution shell in parenthesis).

